SUPPORTING INFORMATION

Small Changes in Hydration Determine Cephalosporinase Activity of OXA-48 β-lactamases

Viivi H. A. Hirvonen[a,b], Adrian J. Mulholland[b], James Spencer[c] and Marc W. van der Kamp[a,b]*

[a] School of Biochemistry, University of Bristol, University Walk, Bristol, BS8 1TD, UK;

Tel: +44 117 331 2147, Fax: +44 17 331 2168.

[b] Centre for Computational Chemistry, School of Chemistry, University of Bristol, Cantock's Close, Bristol, BS8 1TS, UK.

[c] School of Cellular and Molecular Medicine, University of Bristol, University Walk, Bristol, BS8 1TD, UK.

*marc.vanderkamp@bristol.ac.uk

System Set-up and Parameterisation

OXA-48 with ceftazidime was originally set-up using OXA-48 acylenzyme structure with imipenem as the template (PDB:5QB4)[1], and by replacing imipenem with ceftazidime as found in OXA-225 K82D structure (PDB: 4X55)[2]. Upon the publication of OXA-48 P68A with ceftazidime crystal structure (PDB: 6Q5F),[3] further models were built based on the new binding pose of ceftazidime either by taking the new binding pose and combining it with the protein structure used with the first model (with the Ω-loop and β5-β6 loops as found in the apoenzyme), or by mutating the new crystal structure back to the wild-type enzyme and reconstructing the Ω-loop in a disordered state using Modeller (described below). For OXA-163 models, the apoenzyme crystal structure (PDB: 4S2L)[4] was used with both CTZ binding poses. For OXA-181, four residues were mutated with respect to the OXA-48 model, all mutations were performed using the mutagenesis wizard in PyMol (OXA-181 and OXA-48 Arg214Ser). DW was manually added to the active site for all models, and all crystallographic water molecules were kept excluding the ones clashing with the acylenzyme (closer than 2.5 Å from any acylenzyme atom). Carboxylated lysine (Lys73) was kept as found in the OXA-48 and imipenem structure, which is essentially the same as in the OXA-48 apoenzyme structure (PDB: 4S2P)[5]. To avoid any possible steric clashes between the acylenzyme and the rest of the protein, Arg214 was rotated towards bulk solvent in all starting structures. All starting structures are

available to download from Supporting Information as a zip file. Ceftazidime in the acylenzyme was modelled without the pyridine ring, as its elimination has been observed experimentally.[6]

Protonation states of titratable residues were determined using PropKa3.1.[7, 8] Based on the predicted pKa values, all titratable residues were kept in their default state (all Glu/Asp deprotonated, all Lys protonated). Histidine tautomers were predicted using reduce as implemented in the Amber program package (all histidines were singly protonated, are solvent exposed and distant from the active site). Hydrogen atoms were then added and all systems were solvated in a 10 Å box of TIP3P water using tLeap, with overall charge neutralized by replacing bulk water molecules with Na^+ ions. The ff14SB force field was used to describe the protein, and the TIP3P compatible parameters were used for the counterions.[9] Charge parametrization for non-standard residues (carboxylated lysine, KCX, and ceftazidime acylenzyme, CTZ – without the pyridine ring) was done using restrained electrostatic potential (RESP) fitting as implemented in the RED Server.[10] Missing force field parameters were taken from analogous GAFF parameters.[11] Parameter files for both fragments are available as part of the Supporting information zip file.

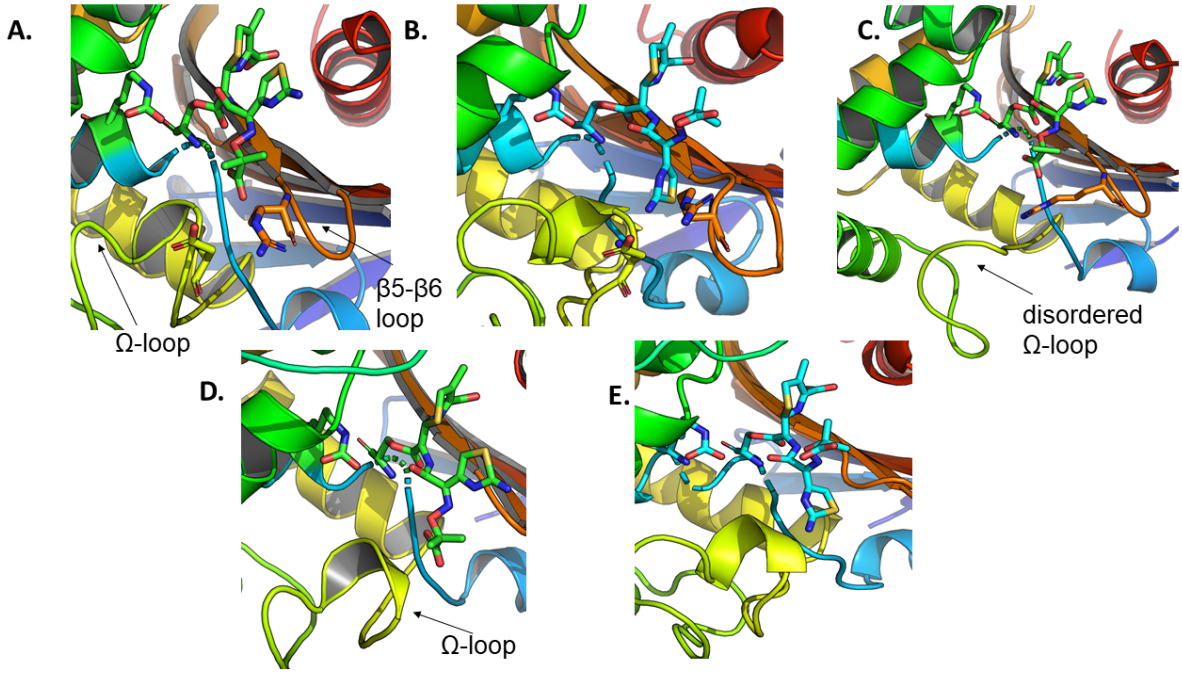

Figure S1*. Different models built for OXA-48 and OXA-163 with ceftazidime. A. OXA-48 with Ω-loop as found in the apoenzyme and ceftazidime binding pose as in the OXA-48 and ceftazidime crystal structure (binding pose 1). B. OXA-48 with Ω-loop as found in the apoenzyme and ceftazidime binding pose as in the OXA-225 and ceftazidime complex (binding pose 2). C. OXA-48 with a disordered Ω-loop built using MODELLER and ceftazidime binding pose as in the OXA-48 and ceftazidime complex. D. OXA-163 and ceftazidime binding pose as in the OXA-48 and ceftazidime crystal structure (binding pose 1). E. OXA-163 and ceftazidime binding pose as in the OXA-225 and ceftazidime structure (binding pose 2).*

Loop Generation

In the OXA-48 structure complexed with CTZ (PDB ID: 6Q5F),[3] electron density was not found for residues between Asp148 and Ile162 (ISGNVDSFWLDGGIR, 13 residue gap). 250 new models for the "disordered" Ω-loop were reconstructed using MODELLER[12] with slow loop refinement, whilst the rest of the atoms in the apoenzyme were kept fixed. (KCX was mutated back to lysine and CTZ

removed for model generation to avoid parameter problems with non-standard residues.) Models were initially inspected using both the DOPE and molpdf scores, and 25 models were chosen for visual inspection (all models were in the top 50 for at least one scoring method, emphasis was given for DOPE scores to include more realistic loop conformations). The final loop model was chosen based on the following criteria: loop residues do not clash with bound ceftazidime in the active site, the new loop does not form interactions with Arg214, and loop reaches in the cavity near the active site (where the "ordered" loop is in the apoenzyme) rather than fully into bulk solvent. All crystallographic waters closer than 2.5 Å to the new loop were deleted to avoid possible clashes.

The "disordered" Ω-loop is not seen in the crystal structure of OXA-48 and ceftazidime (lacking electron density), and it is therefore predicted to be highly flexible compared to the surrounding structural elements. The chosen loop model was validated by measuring Cα-atom RMSF values for three 100 ns molecular dynamics simulations and by comparing the calculated fluctuations of the new Ω-loop against fluctuations in rest of the protein. The first 10 ns of each simulation were excluded from RMSF calculations to allow for system equilibration. RMSF values for each simulation are presented in Figure S2, and they indicate that the newly constructed loop region is the most flexible part of the protein. Loop flexibility is somewhat exaggerated in simulation 2, as it is observed to move into bulk solvent and then move back to the vicinity of the active site.

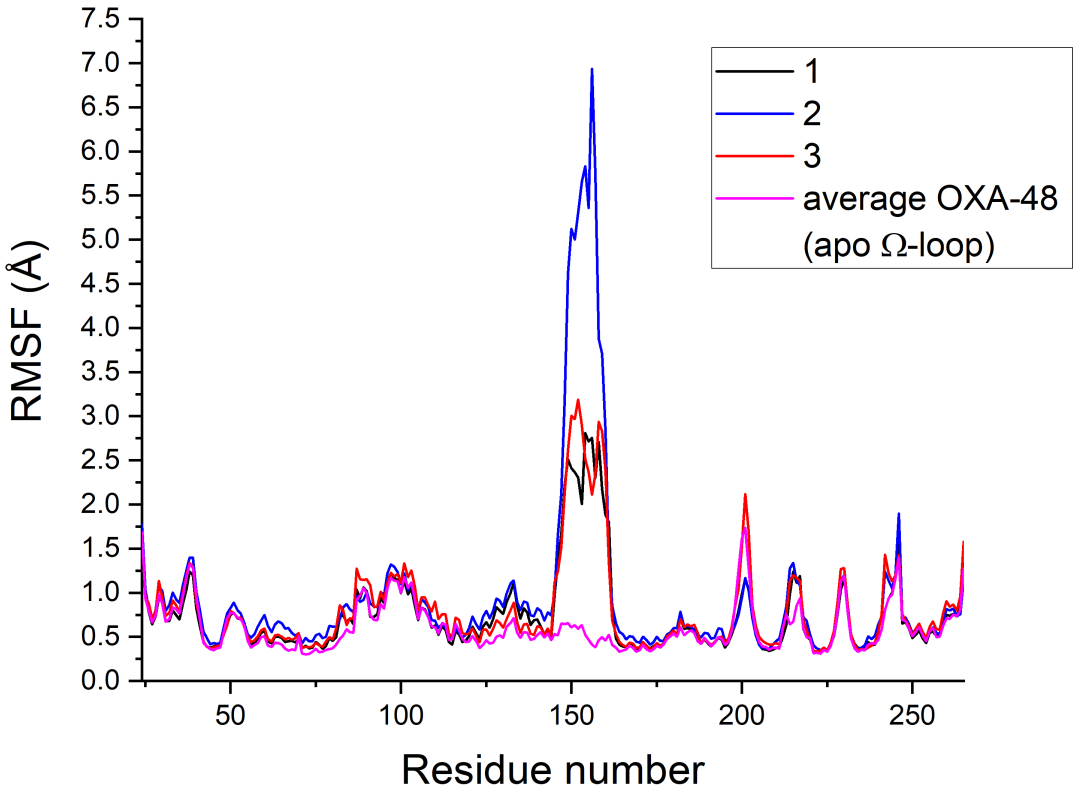

***Figure S2**. RMSF measurement for Cα-atoms for the distorted Ω-loop model of OXA-48. RMSF was measured from three 100 ns MD simulations and compared against the average RMSF for OXA-48 with the apo Ω-loop (magenta, average RMSF taken from five 100 ns MD simulations).*

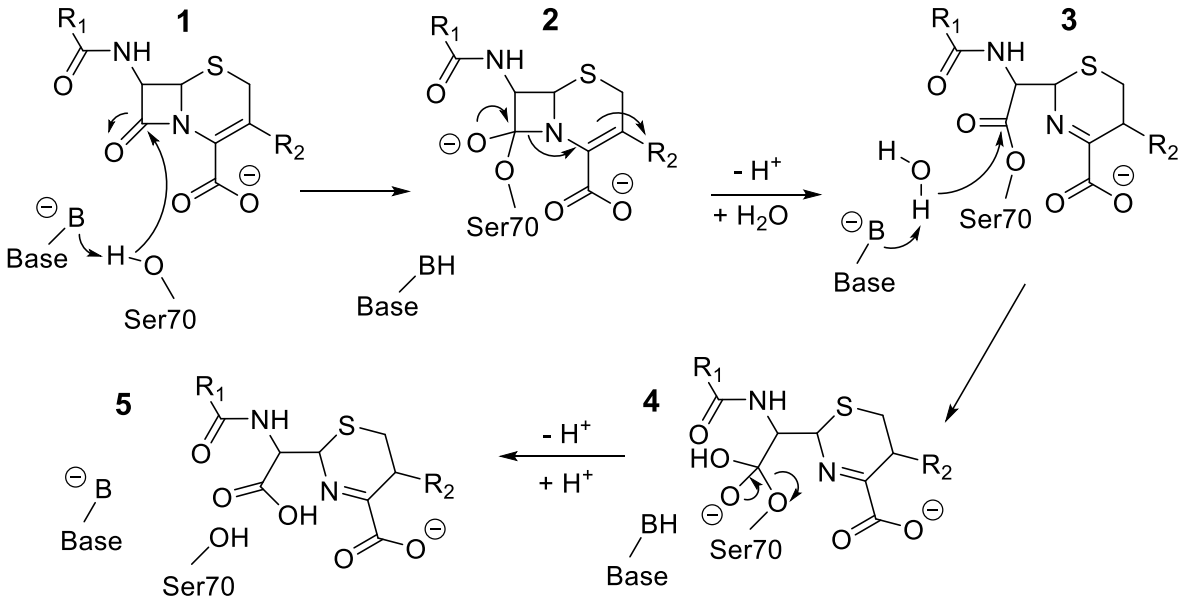

Scheme S1. Schematic illustration of the complete hydrolysis reaction in serine β-lactamases.[13] After the initial Michaelis complex formation, the antibiotic is acylated (1) and a tetrahedral intermediate is formed (2), which collapses to give the acylenzyme structure (3). Subsequently, the acylenzyme is deacylated forming a second unstable tetrahedral intermediate (4), which collapses to the final hydrolysis product (5).

Computational Methods

After initial preparation, all structures were briefly minimized (1000 and 1000 steps of deepest descent and conjugate gradient, respectively) and heated from 50 K to 300 K in 20 ps. After heating, 1 ns MM MD was run to generate starting structures for umbrella sampling (US) calculations. Classical MD simulations were run using Langevin dynamics with a 2 fs timestep constraining all bonds involving hydrogen atoms with the SHAKE algorithm. All starting structures were chosen from the last 500 ps of the 1 ns run to allow for system equilibration during the first half (starting structures at least 50 ps apart). (Tests were also performed using starting structures after at least 50 ns of MM MD, see section "*Extended MD Simulations: Stability, Loop Conformation and Free Energy Barriers*".) All MM MD simulations were performed using a 2 fs timestep, Langevin dynamics with a collision frequency of 0.2, and periodic boundary conditions. The SHAKE algorithm was applied for all bonds involving hydrogen atoms. QM/MM simulations were performed under the same conditions, but with a 1 fs timestep and SHAKE turned off for the QM region. The Amber program package was used for all calculations.[14]

QM/MM Free Energy Calculations

QM/MM US[15, 16] MD simulations were done using two analogous reaction coordinates as for class A enzymes: one for describing the proton transfer from DW to the general base, and one for describing the nucleophilic attack (Figure S3). The proton transfer reaction coordinate was sampled from 1.0 to −1.0 Å, and the nucleophilic attack coordinate from 3.8 to 1.4 Å, both in 0.1 Å increments with a 100 kcal mol^{-1} $Å^{-2}$ force constant. First, US was performed along an approximate (see below) minimum

free energy path (MFEP) from AE to TI on the 2D free energy surface (FES) in 33 US windows, and afterwards sampling along the rest of the surface was performed using these windows as starting points (altogether 525 US windows). US was first done for in each window for 2 ps for equilibration, followed by a further 20 ps along the approximate MFEP and a further 2 ps in all other windows. This approach should ensure enough sampling near the true reaction path, whilst minimizing sampling in high energy regions on the FES. US was done for four different starting structures taken from a 1 ns MM/MD run. The QM region consists of the deacylating water (DW), KCX, and a part of the covalently bound drug (38 atoms, Figure S4), and DFTB3[17] was used as the QM method with a 1 fs timestep. Covalent bonds between the QM and MM regions were treated using the hydrogen link atom scheme implemented in sander (Amber). A one-sided restraint was added for the ester bond between Ser70 and the substrate to ensure it does not elongate above 1.6 A (Figure S4). All US results were analysed and FESs constructed using WHAM[18] with 21 and 25 bins for the proton transfer and nucleophilic attack coordinates respectively, with a convergence criterium set to $1x10^{-13}$. Calculations were done for four snapshots, and the overall energy barriers were obtained by combining all sampling from these four US calculations into one WHAM calculation. True MFEPs on the FESs were calculated using the Minimum Energy Pathway Analysis for energy landscapes (MEPSA) code.[19]

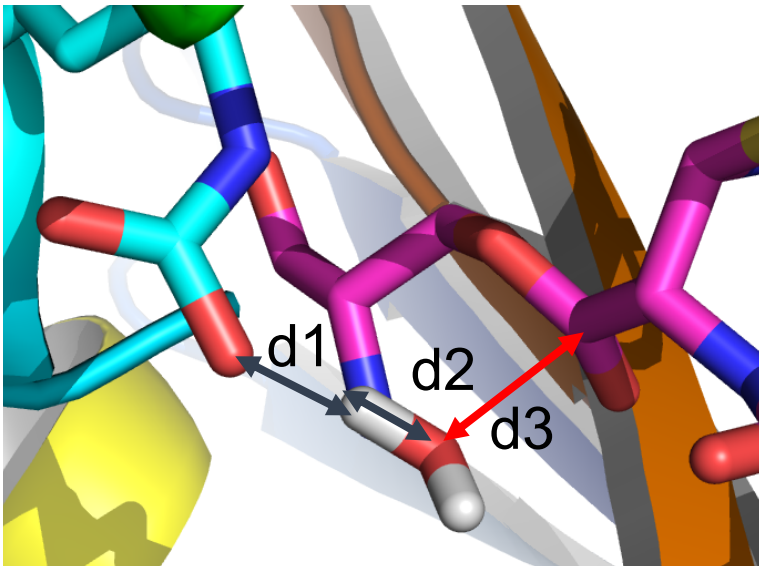

***Figure S3**. Illustration of the reaction coordinates used in umbrella sampling describing the changed in bonding during the tetrahedral intermediate formation. The proton transfer coordinate is defined with dark blue arrows as the difference d1-d2 (d[Lys73:O, DW:H] – d[DW:O, DW:H]). The nucleophilic attack coordinate is depicted as the red arrow, distance d3 (d[DW:O, CTZ:C]).*

The approximate minimum energy path for OXA-48 variants was constructed based on calculated class A deacylation surfaces, and consists of 33 initial US windows (PT=proton transfer, NA=nucleophilic attack):

PT	1.0	0.9	0.8	0.8	0.8	0.8	0.8	0.8	0.8	0.8	0.8	0.8	0.8	0.7	0.6
NA	3.8	3.7	3.6	3.5	3.4	3.3	3.2	3.1	3.0	2.9	2.8	2.7	2.6	2.5	2.4

PT	0.5	0.4	0.3	0.2	0.1	0.0	-0.1	-0.2	-0.3	-0.4	-0.5	-0.6	-0.7
NA	2.3	2.2	2.2	2.1	2.1	2.0	1.9	1.8	1.7	1.7	1.6	1.6	1.5

PT	-0.8	-0.8	-0.9	-1.0
NA	1.5	1.4	1.4	1.4

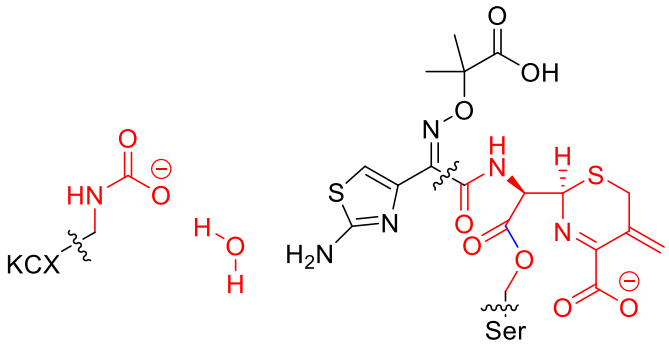

***Figure S4**. QM region used in US calculations; QM atoms in red, MM atoms in black; location of link atoms indicated with squiggly lines. The ester bond in blue was restrained to be less than (or equal to) 1.6 A during US to avoid sampling the next step.*

Free Energy Surfaces – short sampling

Free energy barriers for deacylation ($\Delta^{\ddagger}G_{calc}$ values) in Table 1 (main manuscript) were calculated by sampling 20 ps near the approximate minimum energy path and 2 ps elsewhere on the free energy surface (as described above, from now on referred to as 20 + 2 ps sampling). The 2 ps 'equilibration' sampling in each window (prior to the US used for the free energy analysis reported in Table 1) was also used directly for the calculation of free energy surfaces using WHAM (as detailed above). Notably, $\Delta^{\ddagger}G_{calc}$ values based on the 2 ps surfaces (without equilibration) do not largely differ from the 20 + 2 ps results (largest difference 0.5 kcal/mol; see Table S1), and show the same consistent difference in deacylation rates between different OXA-48 variants.

***Table S1**. Deacylation free energy barriers calculated from 2 ps sampling. All values in kcal/mol, standard deviations in parenthesis.*

Enzyme	k_{cat} **(s^{-1})**[20]	**$\Delta^{\ddagger}G_{calc}$ (kcal/mol)**		
		Binding pose 1	Binding pose 2	New Ω-loop
OXA-48	NH	12.4 (0.8)	18.5 (1.0)	>20[a]
OXA-48 R214S	-	6.9 (0.5)	14.0 (1.4)	>20[a]
OXA-163	8	7.2 (0.3)	15.7 (1.4)	N/A
OXA-181	ND	11.0 (1.9)	17.7 (0.6)	-
OXA-181 R214S	-	6.4 (0.3)	N/A	-

NH = No hydrolysis detected. ND = Not determined. N/A = Not applicable (Ω-loop not present).

[a] transition state could not be located on the free energy surface, with energy values rising to above 20 kcal/mol near the TI

Benchmarking

For the QM/MM MD umbrella sampling simulations, the semi-empirical DFTB3 method was used. The free energy surface indicates a concerted mechanism with a barrier lower than that expected from experiment. Here, we perform more accurate DFT calculations (and *ab initio* single-point energy calculations) using a small gas-phase system representing the quantum region used in our QM/MM simulations (Figure S5). Transition states (TS) were optimised on both the M06-2X/6-31+G(d)[21, 22] and BLYP/6-31G+(d)[23, 24] levels using the QST3 algorithm as implemented in Gaussian09[25]. UltraFine integration grid was used for all calculations.

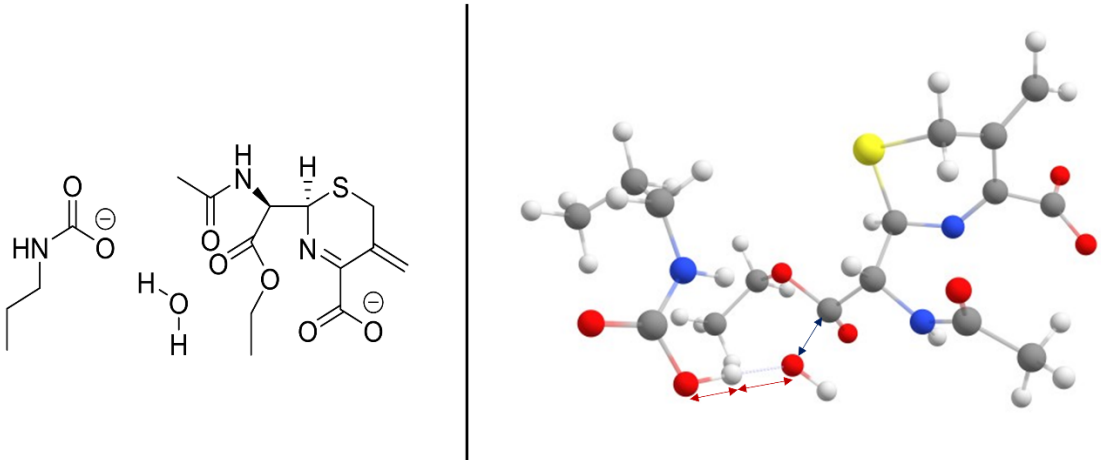

Figure S5. *Left: Small molecule model representing the QM region used in benchmarking calculations. Right: M06-2X/6-31+G(d) optimized transition state of the small molecule model. Red arrows: proton transfer reaction coordinate, blue arrow: nucleophilic attack reaction coordinate.*

TSs were characterized by a frequency calculations, and the TS on the M06-2X level corresponded to one imaginary frequency (-293.2677), whilst TS optimized using the BLYP functional yielded two imaginary frequencies (-107.3119 corresponding to the reaction, and one at -1.8944, corresponding to an overall bend/twist motion). IRC calculations starting from the M06-2X TS structure were performed in both directions to obtain the reactant and product minima, and the end structures where further optimised on the M06-2X/6-31+G(d) level. Reactants and products were optimised also with BLYP (starting from the M06-2X optimised structures). The reaction coordinate values of the TSs indicate that the reaction proceeds through a concerted mechanism, similar to that predicted by the DFTB3/ff14SB free energy surface (Table S2). Calculated activation energies (Table S2) indicate that DFTB3 significantly underestimates this value. RI-SCS-MP2/aug-cc-pVTZ[26-28] single-point energies were calculated on the M06-2X optimized structures using Orca 4.2[29, 30] (using the RIJK approximation and aug-cc-pVTZ/C and aug-cc-pVQZ/JK auxiliary basis sets[31]). DFTB3 single-point energies were calculated for BLYP optimized structures using sqm as part of the Amber package.[15] Comparison of these RI-SCS-MP2/aug-cc-pVTZ and DFTB3 activation energies shows that, based on these potential energies only, DFTB3 underestimates the activation energy by 7 kcal/mole.

***Table S2**. Location of the transition state for M06-2X and BLYP optimized small QM model (Figure S5), and calculated activation energy barrier. NA RC = nucleophilic attack reaction coordinate, PT RC = proton transfer reaction coordinate.*

Method	NA RC (Å)	PT RC (Å)	$\Delta^{\ddagger}G_{calc}$ (kcal/mol)
M06-2X/6-31+G(d)	1.97	-0.35	14.85
RI-SCS-MP2/aug-cc-pVTZ[a]	-	-	16.63
BLYP/6-31+G(d)	1.83	-0.51	15.53
DFTB3[b]	-	-	9.65
DFTB3/ff14SB FES (OXA-48)[c]	1.7	-0.5	

[a] Energy difference from single-point energies on M06-2X/6-31+G(d) optimized AE and TS structures.

[b] Energy difference from single-point energies on BLYP/6-31+G(d) optimised AE and TS structures; A transition state could not be optimized in the gas-phase with DFTB3 as no saddle point is indicated between the AE minimum and the tetrahedral intermediate.

[c] For reference, the approximate TS location obtained from the QM/MM free energy surface (see Figure 2) is indicated.

For the purpose of comparing the in-enzyme energy surface shape and energies, a QM/MM potential energy surface was obtained. Starting from a snapshot of one OXA-48 US simulation in the window corresponding to the (approximate) transition state, a potential energy surface (PES) was calculated for the deacylation reaction. The LBFGS method was used for minimization (with convergence criterium of 0.01 mol^{-1} $Å^{-1}$ for energy gradients). Residues further than 5 Å away from ceftazidime were restrained with a restraint weight of 50 kcal mol^{-1} $Å^{-2}$ (to avoid discontinuities). Single-point energy corrections were calculated by taking the difference in the QM region energies calculated at the M06-2X/def2-TZVP level (using the RIJK approximation with def2/JK auxiliary basis set) with Orca 4.2 and the DFTB3 level. (QM-MM interaction terms were thus calculated with DFTB3.)

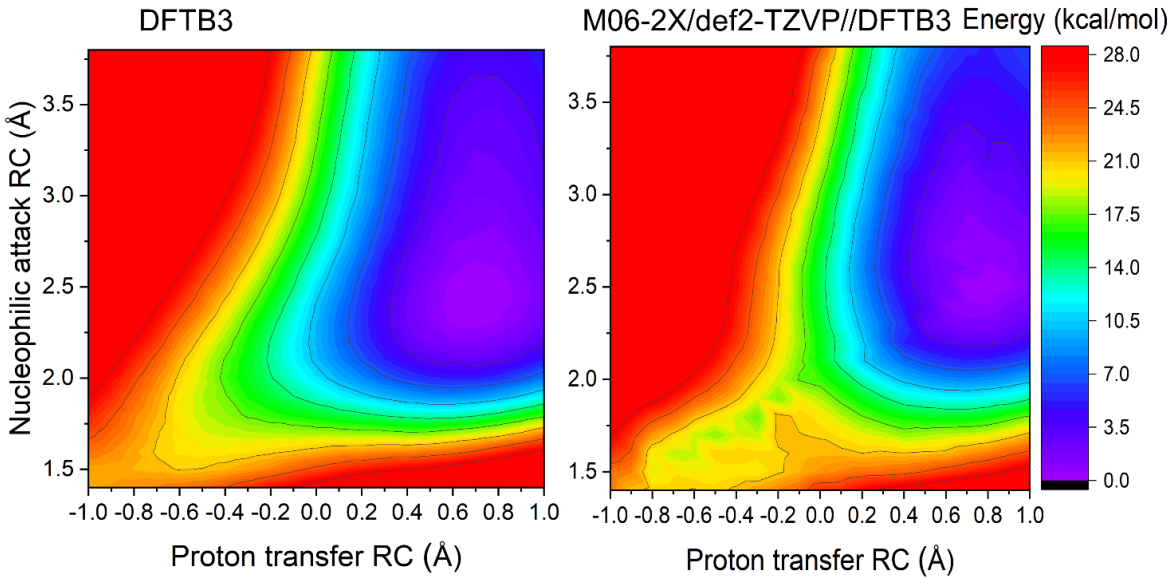

***Figure S6.** Left: Potential energy surface for ceftazidime deacylation calculated with DFTB3; energy at -0.5,1.6 (location of the free energy surface TS) is 13.4 kcal/mole. Right: DFTB3 potential energy surface with M06-2X/def2-TZVP energy corrections; approximate TS at -0.3,1.9 is 19.4 kcal/mole. The difference of 6 kcal/mole is in line with the small model calculations (Table S2).*

Mulliken Charge Calculations

Mulliken charges for the QM region were calculated from extended US in both acylenzyme and tetrahedral intermediate minima from one individual US free energy surface. Charge values were calculated as an average from 1000 frames over 20 ps (i.e. snapshots recorded every 20 fs). Mulliken charges are presented for OXA-48 (both ordered and disordered Ω-loop), OXA-48 Arg214Ser, and OXA-163. All four models show the same trend, where largest charge variations are observed for the atoms that directly take part in deacylation or are near the reactive parts (Figure S7). Mulliken charges were recorded for the QM atoms in both the enzyme environment and in the gas-phase. For the gas-phase charge calculations, each frame of the QM/MM MD trajectory was extracted as a separate structure and pseudo-minimized (minimization with 0 steps) to obtain the QM region with link atoms. Subsequently, a single-point QM calculation was done for each QM region structure using sqm (as implemented in Amber) to obtain the Mulliken charges. The results on key atoms are reported in Tables S3-S5.

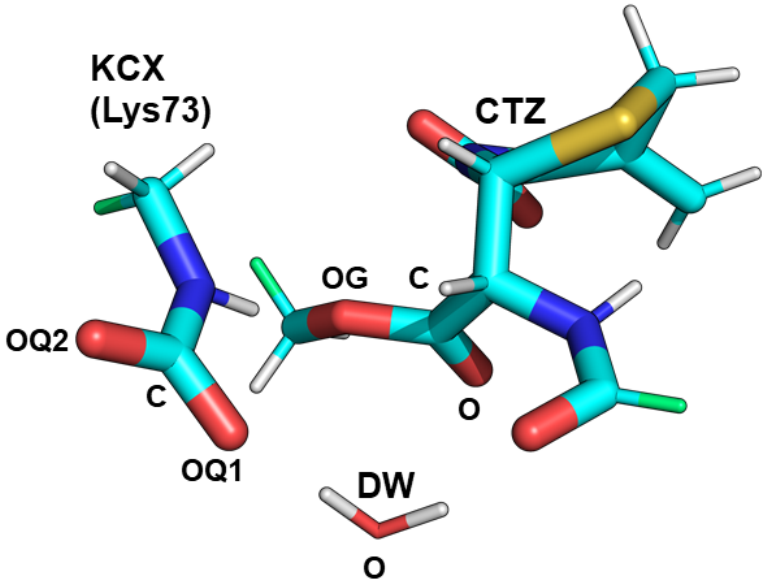

***Figure S7**. QM region with link atoms (in green). Atom names shown for selected heavy atoms, whose Mulliken charges were recorded during QM/MM MD.*

***Table S3**. Mulliken charges for WT OXA-48 and ceftazidime.*

QM atom	Enzyme			QM region only		
	Q^{AC}	Q^{TI}	ΔQ^{TI-AC}	Q^{AC}	Q^{TI}	ΔQ^{TI-AC}
KCX-OQ1	-1.01	-0.59	0.41	-0.93	-0.56	0.36
KCX-OQ2	-0.91	-0.80	0.11	-0.86	-0.74	0.12
KCX-C	0.98	0.83	-0.15	0.94	0.81	-0.13
DW-O	-0.85	-0.76	0.09	-0.84	-0.73	0.11
CTZ-O	-0.65	-1.0	-0.35	-0.56	-0.92	-0.37
CTZ-C	0.71	0.91	0.20	0.69	0.89	0.20
CTZ-OG	-0.34	-0.59	-0.26	-0.34	-0.6	-0.26

***Table S4**. Mulliken charges for WT OXA-48 with a 'disordered' Ω-loop and ceftazidime.*

QM atom	Enzyme			QM region only		
	Q^{AC}	Q^{TI}	ΔQ^{TI-AC}	Q^{AC}	Q^{TI}	ΔQ^{TI-AC}
KCX-OQ1	-1.03	-0.64	0.39	-0.92	-0.59	0.32
KCX-OQ2	-0.95	-0.85	0.10	-0.87	-0.76	0.11
KCX-C	1.00	0.87	-0.14	0.93	0.82	-0.11
DW-O	-0.89	-0.75	0.14	-0.88	-0.71	0.17
CTZ-O	-0.69	-0.99	-0.30	-0.60	-0.91	-0.31
CTZ-C	0.74	0.91	0.17	0.71	0.88	0.18
CTZ-OG	-0.33	-0.57	-0.25	-0.33	-0.58	-0.25

***Table S5**. Mulliken charges for R214S OXA-48 and ceftazidime.*

QM atom	Enzyme			QM region only		
	Q^{AC}	Q^{TI}	ΔQ^{TI-AC}	Q^{AC}	Q^{TI}	ΔQ^{TI-AC}
KCX-OQ1	-0.94	-0.59	0.35	-0.89	-0.56	0.33
KCX-OQ2	-0.89	-0.78	0.11	-0.86	-0.74	0.12
KCX-C	0.96	0.83	-0.14	0.94	0.81	-0.13
DW-O	-0.93	-0.79	0.14	-0.87	-0.76	0.11
CTZ-O	-0.69	-1.00	-0.31	-0.56	-0.88	-0.32
CTZ-C	0.73	0.93	0.20	0.70	0.91	0.21
CTZ-OG	-0.32	-0.60	-0.27	-0.34	-0.62	-0.28

***Table S6**. Mulliken charges for OXA-163 and ceftazidime.*

QM atom	Enzyme			QM region only		
	Q^{AC}	Q^{TI}	ΔQ^{TI-AC}	Q^{AC}	Q^{TI}	ΔQ^{TI-AC}
KCX-OQ1	-0.94	-0.61	0.33	-0.90	-0.59	0.32
KCX-OQ2	-0.89	-0.79	0.10	-0.86	-0.75	0.11
KCX-C	0.97	0.84	-0.13	0.94	0.82	-0.12
DW-O	-0.92	-0.82	0.10	-0.88	-0.81	0.06
CTZ-O	-0.67	-1.00	-0.33	-0.57	-0.90	-0.33
CTZ-C	0.73	0.92	0.20	0.70	0.90	0.21
CTZ-OG	-0.32	-0.53	-0.21	-0.33	-0.54	-0.21

Acylenzyme Clustering

Clustering of the acylenzyme was done based on five 50 ns MD simulations (1250 frames/simulation) per acylenzyme model (OXA-48 with (dis)ordered Ω-loop, OXA-48 Arg214Ser, OXA-163). All MD simulations were combined into one clustering calculation by stripping all solvent molecules and parts of the protein that did not match between all enzymes (e.g β5 - β6 loop in OXA-48). Trajectories were aligned based on Cα-atoms of 12 residues near the active site (CTZ, Thr71-Pro75, Ser118, Lys208-Tyr211, Lys218), and the substrate orientations were clustered into four clusters (using a sieve of 20) based on the RMSD of CTZ heavy atoms. The clustering analysis does not show any significant differences between the different enzyme models near the formed ester bond and the electrophilic carbon, but larger deviations between enzymes are seen for the oxyimino and thiazole groups. As depicted in Figure S8, OXA-48 with a newly constructed Ω-loop is seen to sample one orientation not observed for other enzymes (green cluster), as it has more space in the active site for substrate movement due to loop distortion.

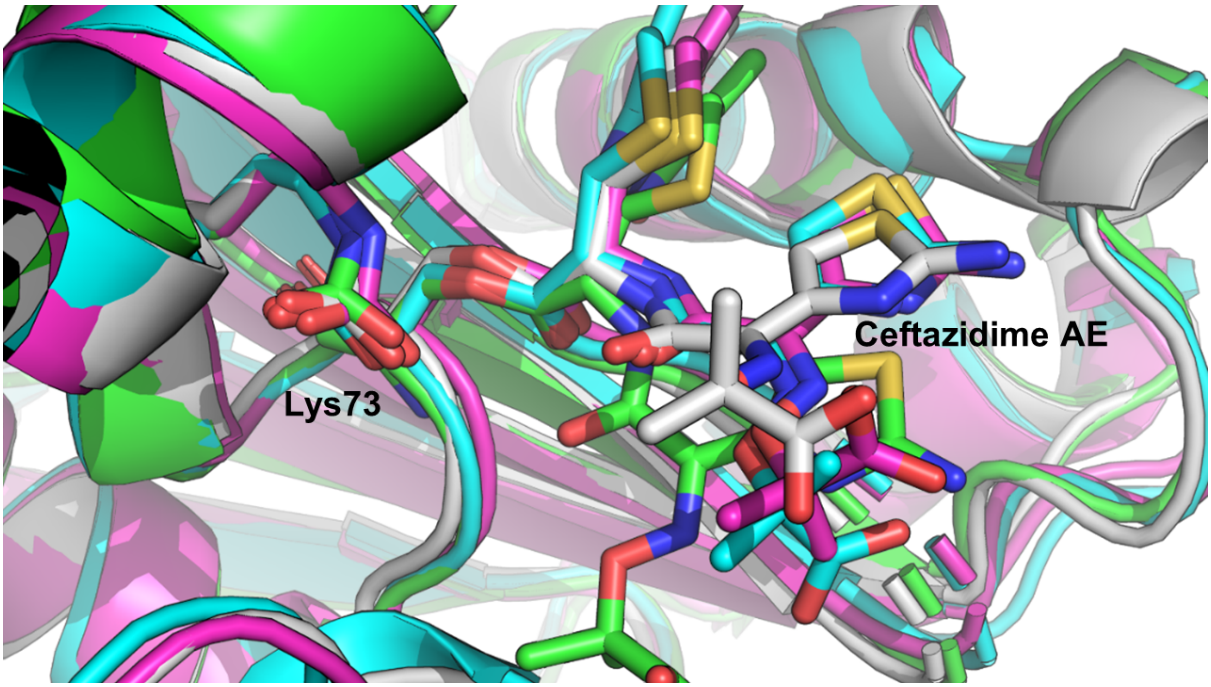

Figure S8. *Acylenzyme orientations during extended MD from k-means clustering analysis. Representative structures (cluster centroids) are shown of the largest clusters (most sampled orientations) for OXA-48 (grey), OXA-163 (magenta), OXA-48 Arg214Ser (cyan), and OXA-48 with distorted Ω-loop (cyan & green).*

Oxyanion Hole Hydrogen Bond Distances

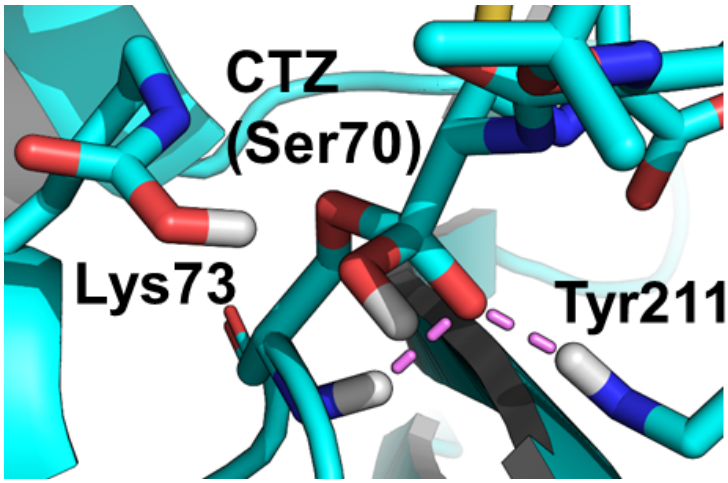

***Figure S9**. The oxyanion hole, formed by backbones of Ser70 (the AE) and Tyr211, stabilises the formation of a tetrahedral intermediate (hydrogen bonds highlighted in violet).*

Because oxyanion hole interactions are known to stabilise the forming tetrahedral intermediate structure, distances of these hydrogen bonds (formed by the backbones of Ser70 in the ceftazidime acylenzyme and Tyr211, Figure S9) were measured both from five 50 ns MM MD simulations per enzyme (for the acylenzyme), and from four 20 ps QM/MM MD simulations per enzyme (for the tetrahedral intermediate). Distance measurements are presented in Figures S10-S13. Overall, distances are very similar, and do not correlate with differences in the reaction barrier between the different enzyme models.

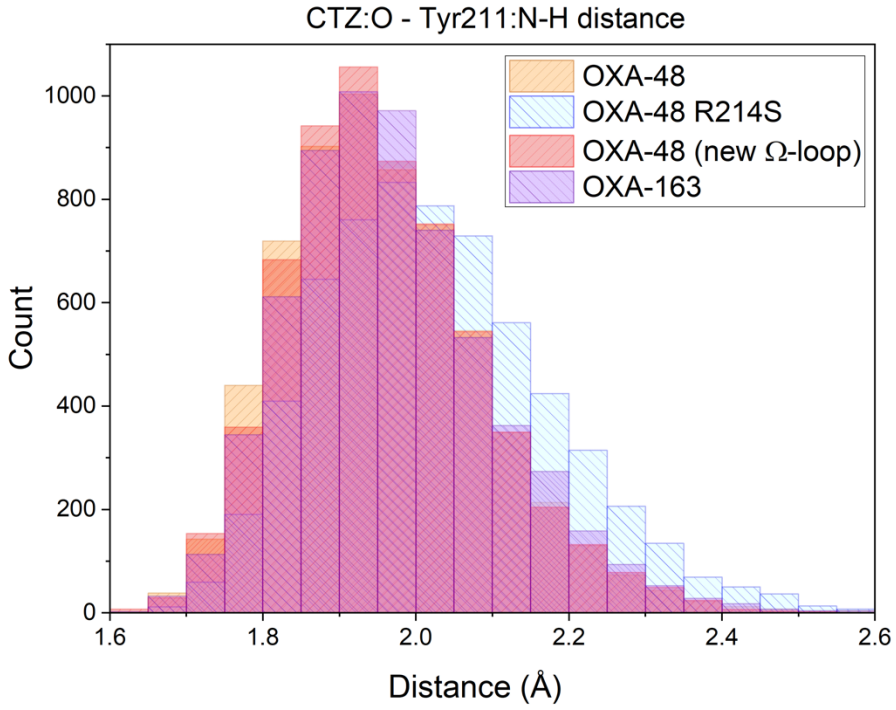

***Figure S10**. Hydrogen bond distances between the mainchain of Tyr211 and ceftazidime in the oxyanion hole from 50 ns MM/MD (measured from five MD simulations per acylenzyme model).*

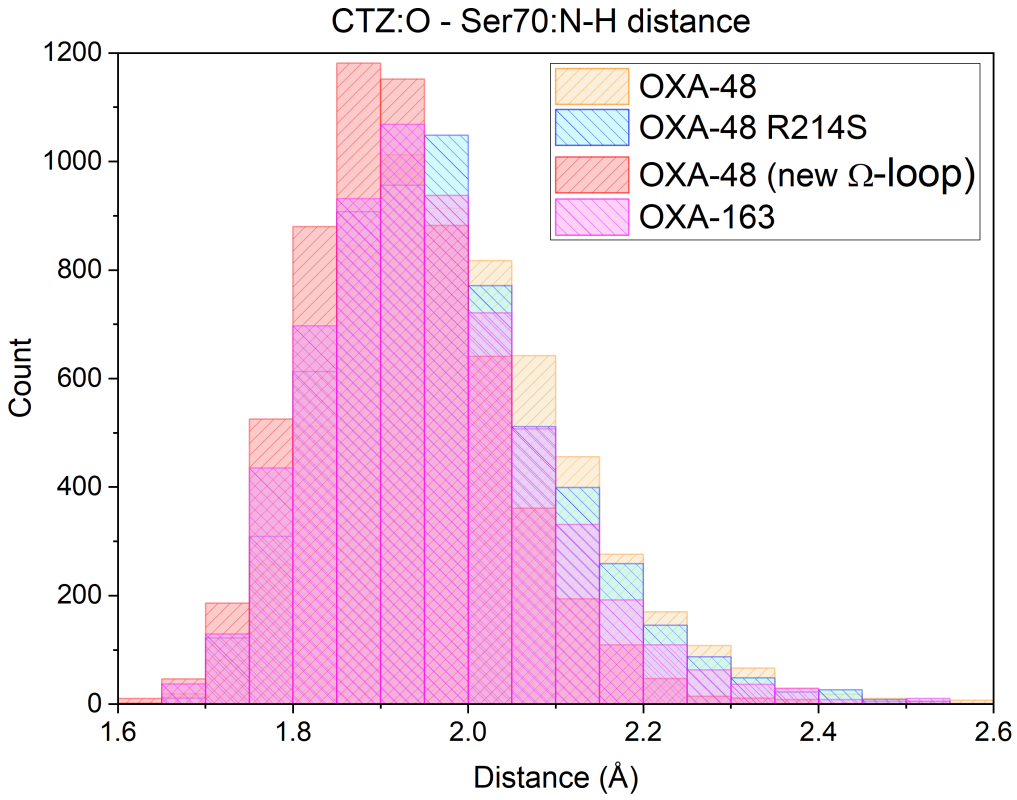

Figure S11. *Hydrogen bond distances between the mainchain of Ser70 and ceftazidime in the oxyanion hole from 50 ns MM/MD (measured from five MD simulations per acylenzyme model).*

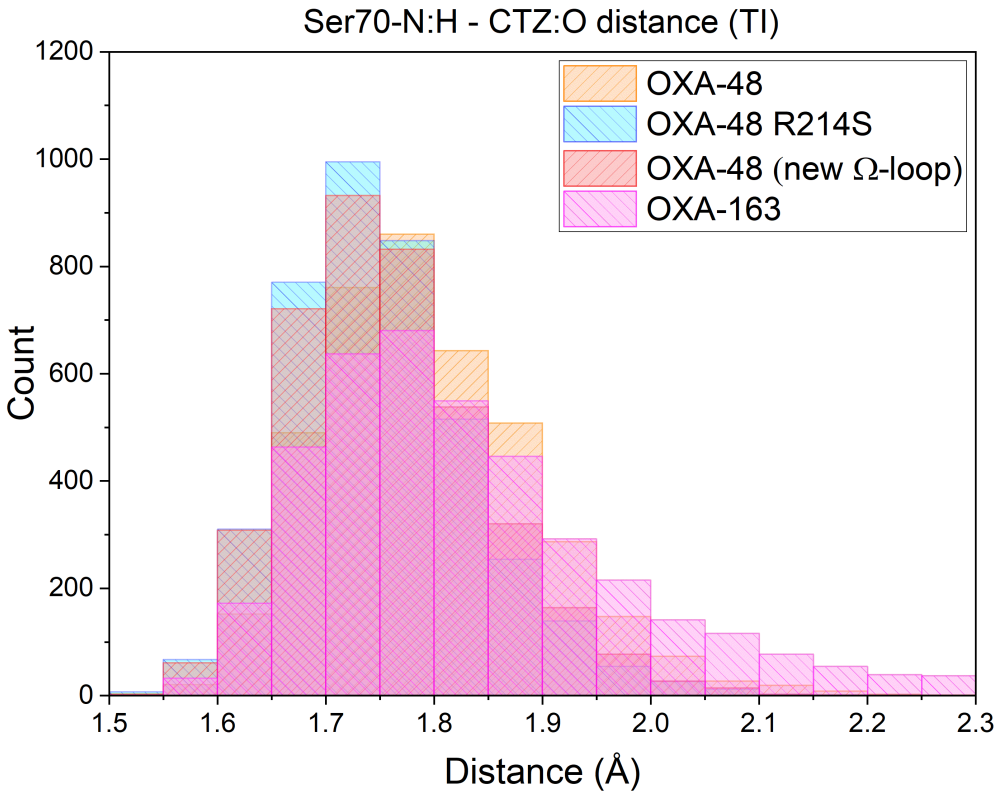

Figure S12. *Oxyanion hole distances between Ser70 backbone and ceftazidime in the tetrahedral intermediate from 20 ps QM/MM MD.*

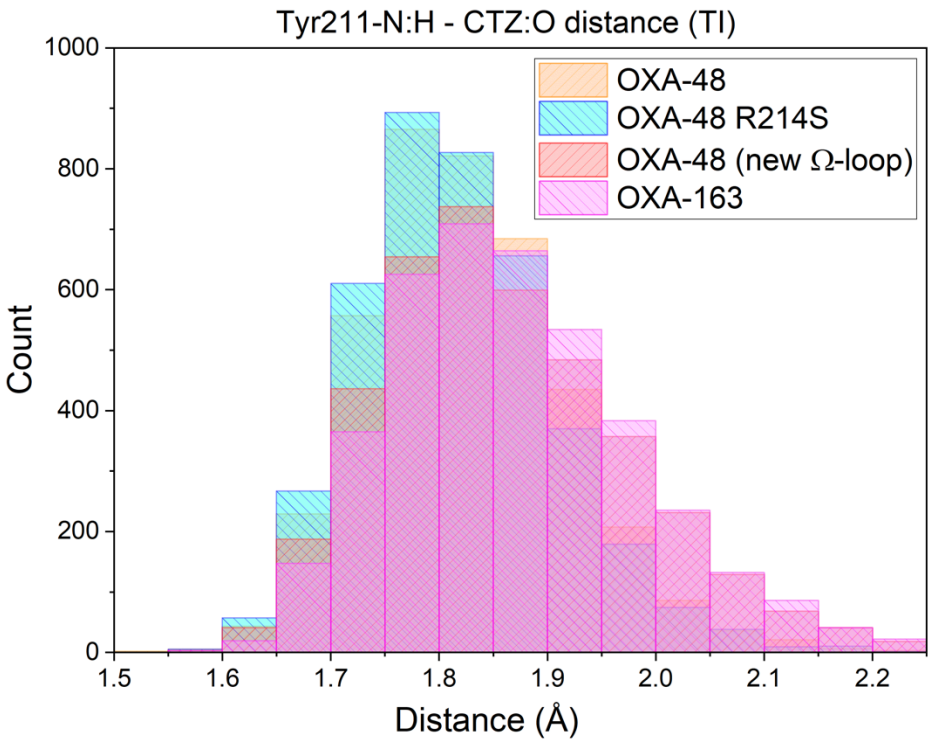

Figure S13. *Oxyanion hole distances between Tyr211 backbone and ceftazidime in the tetrahedral intermediate from 20 ps QM/MM MD.*

Leu158 Rotation

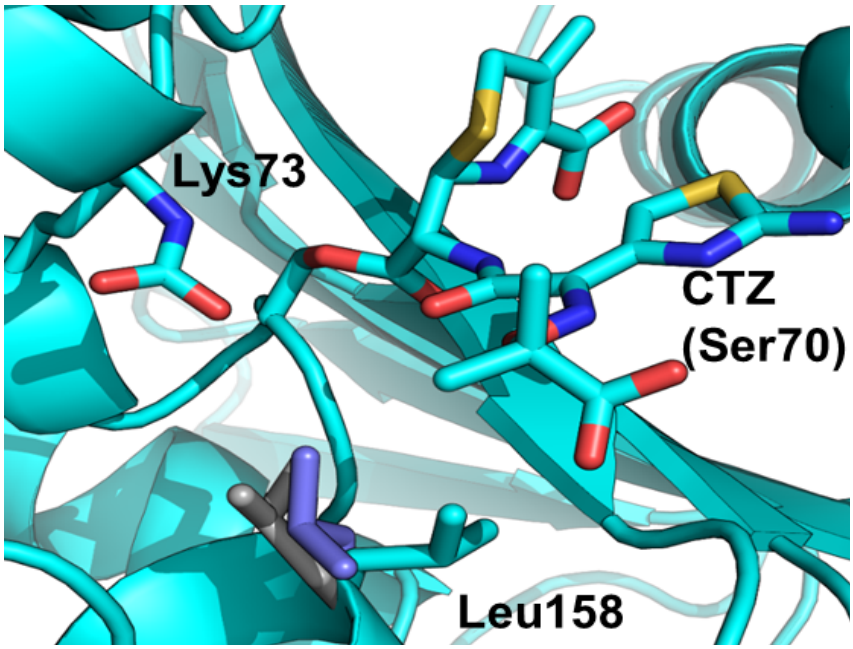

Figure S14. *Three observed rotamers of Leu158. Representative structures are highlighted for structures where the C-Cα-Cβ-Cγ dihedral angle (χ_1) is approximately 50° (g+; cyan), 170° (t; grey), and 290° (g-; purple).*

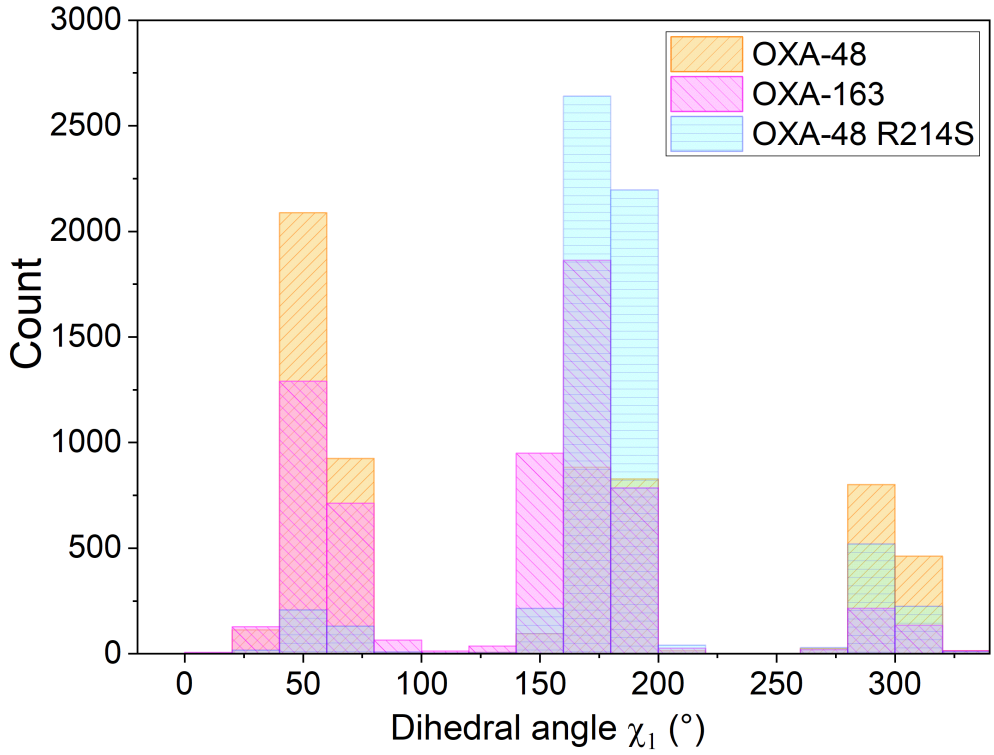

Figure S15. *Leu158 C-Cα-Cβ-Cγ dihedral (χ_1) values measured from five 50 ns MD simulations for each enzyme. Three different rotamers are observed for each enzyme during MD simulations: around 50°, 170° and 290° (g+, t, and g-, respectively). The orientation found in the apoenzyme corresponds to the 170° orientation, and the two different orientations mainly occur for OXA-48.*

Extended MD Simulations: Stability, Loop Conformation and Free Energy Barriers

To further inspect the stability of the simulation systems and check for possible of conformational changes in the studied OXA-48 variants, we ran five additional independent 120 ns MD simulations each for the acylenzymes of OXA-48, OXA-163 and OXA-48 R241S (in binding mode 1 and with the ordered Ω-loop). Measurement of the RMSD for Cα-atoms (excluding the first flexible five residues in the N terminus) indicates that all three systems are stable (Figure S15).

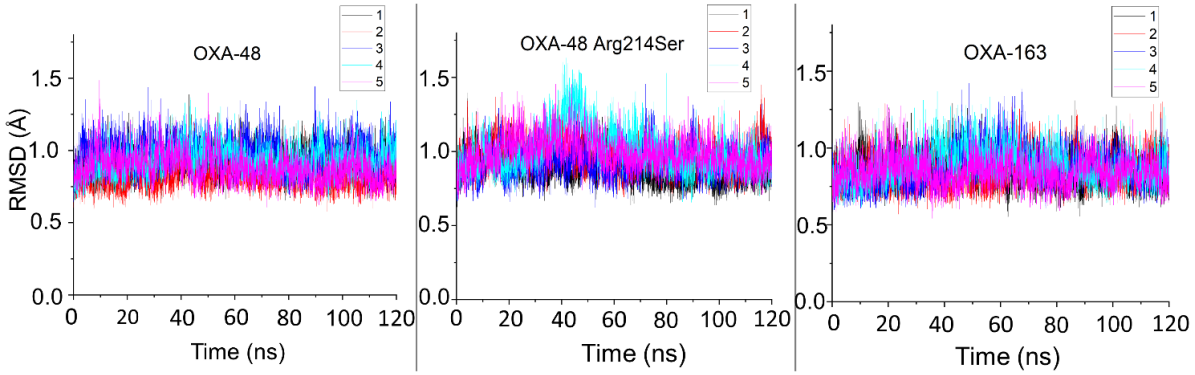

Figure S16. *Cα-RMSD of five 120 ns MM MD simulations for OXA-48 (left), OXA-48 Arg214Ser (middle), and OXA-163 (right)*

.

The β5 – β6 loop movement in OXA-48 and OXA-48 R214S was further inspected from the 120 ns MD simulations by clustering the sampled loop orientations based on Cα-RMSD. All five OXA-48 trajectories and five OXA-48 R214S trajectories were aligned on Cα-atoms of residues 29-211 & 219-265 (excluding five residues from the N-terminal end), and then divided in 5 clusters based on Cα-RMSD of the β5 – β6 loop (residues 212-218). Clustering was performed with the *k*-means algorithm as implemented in cpptraj with a sieve of 20. For the majority of simulation time, the β5 - β6 loop in OXA-48 and in OXA-48 R214S sample the same conformational space (70% and 76% in clusters 1-3 for OXA-48 and OXA-48 R214S, respectively, with populations ≥ 20% for each enzyme/cluster). Although the remainder of the time (30% and 23% for OXA-48 and OXA-48 R214S, respectively) the loop conformations are slightly different, it is clear that the mutation does not lead to a significant shift to a new conformational state (Figure S16).

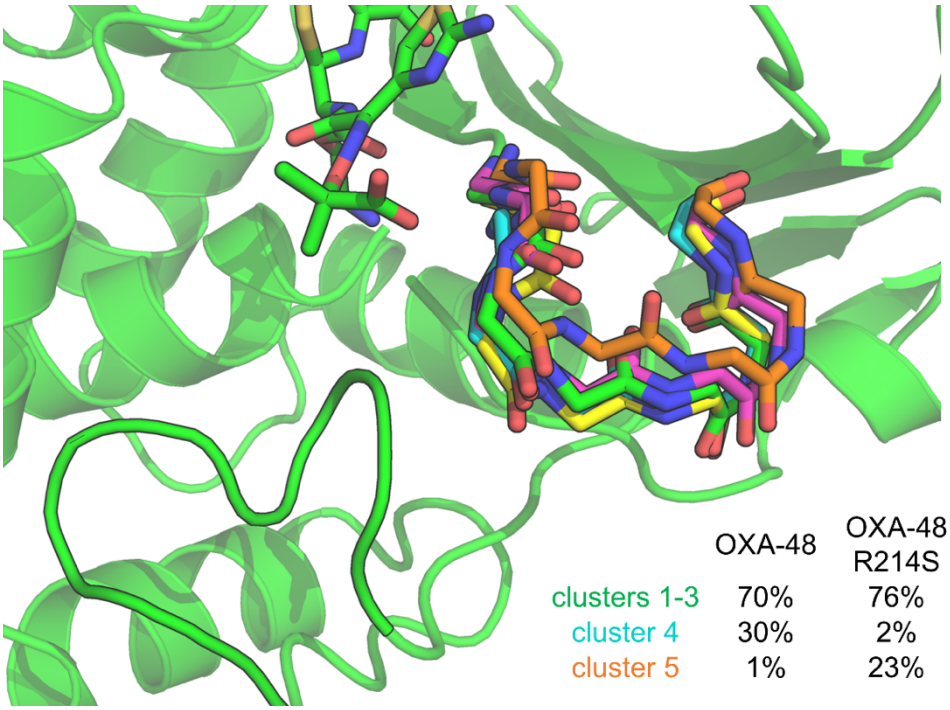

Figure S17. *Clustering of the β5 - β6 loop (k-means clustering based on loop backbone RMSD after alignment on the rest of the protein, into 5 clusters) of 5x 120ns simulations of both OXA-48 and OXA-48 R214S. Loop carbons are coloured by cluster as follows: 1 green, 2 magenta, 3 yellow, 4 cyan and 5 orange. Ceftazidime acylenzyme and the Ω-loop are also shown, for reference.*

Additionally, we performed one QM/MM (DFTB3/ff14SB) US simulation per enzyme variant by taking a starting structure from the 120 ns MD simulations. To make the calculated energetics comparable with the ones calculated for starting structures taken from 1 ns MD simulation, the structure for each variant was chosen so that Leu158 conformation and active site hydration replicate the ones observed in the original starting structures (i.e. Leu158 dihedral is 50° for OXA-48, and 170° for OXA-48 Arg214Ser and OXA-163). Results from 2 ps QM/MM US simulations, using the same procedure as applied previously, indicate similar free energies are obtained as with snapshots from the initial short 1 ns MD simulation (Table S7).

Table S7*. Free energy barriers calculated with DFTB3/ff14SB umbrella sampling from extended MD snapshots.*

Enzyme	**Time**	**$\Delta^{\ddagger}G_{calc}$ (kcal/mol)**
OXA-48	50 ns	12.42
OXA-48 R214S	120 ns	7.45
OXA-163	110 ns	7.93

References

1. Akhter, S.; Lund, B. A.; Ismael, A.; Langer, M.; Isaksson, J.; Christopeit, T.; Leiros, H. S.; Bayer, A., A focused Fragment Library Targeting the Antibiotic Resistance Enzyme - Oxacillinase-48: Synthesis, Structural Evaluation and Inhibitor Design. *Eur. J. Med. Chem.* **2018,** *145*, 634-648.
2. Mitchell, J. M.; Clasman, J. R.; June, C. M.; Kaitany, K. C.; LaFleur, J. R.; Taracila, M. A.; Klinger, N. V.; Bonomo, R. A.; Wymore, T.; Szarecka, A.; Powers, R. A.; Leonard, D. A., Structural Basis of Activity Against Aztreonam and Extended Spectrum Cephalosporins for Two Carbapenem-Hydrolyzing Class D β-lactamases from Acinetobacter baumannii. *Biochemistry* **2015,** *54*, 1976-1987.
3. Fröhlich, C.; Sorum, V.; Thomassen, A. M.; Johnsen, P. J.; Leiros, H. S.; Samuelsen, O., OXA-48-Mediated Ceftazidime-Avibactam Resistance Is Associated with Evolutionary Trade-Offs. *mSphere* **2019,** *4*, e00024-19.
4. Stojanoski, V.; Chow, D. C.; Fryszczyn, B.; Hu, L.; Nordmann, P.; Poirel, L.; Sankaran, B.; Prasad, B. V.; Palzkill, T., Structural Basis for Different Substrate Profiles of Two Closely Related Class D β-Lactamases and Their Inhibition by Halogens. *Biochemistry* **2015,** *54*, 3370-3380.
5. King, D. T.; King, A. M.; Lal, S. M.; Wright, G. D.; Strynadka, N. C., Molecular Mechanism of Avibactam-Mediated β-Lactamase Inhibition. *ACS Infect. Dis.* **2015,** *1*, 175-184.
6. Vakulenko, S. B.; Taibi-Tronche, P.; Toth, M.; Massova, I.; Lerner, S. A.; Mobashery, S., Effects on Substrate Profile by Mutational Substitutions at Positions 164 and 179 of the Class A TEMpUC19 β-Lactamase from Escherichia coli. *J. Biol. Chem.* **1999,** *274*, 23052–23060.
7. Sondergaard, C. R.; Olsson, M. H.; Rostkowski, M.; Jensen, J. H., Improved Treatment of Ligands and Coupling Effects in Empirical Calculation and Rationalization of pKa Values. *J. Chem. Theory Comput.* **2011,** *7*, 2284-2295.
8. Olsson, M. H. M.; Søndergaard, C. R.; Rostkowski, M.; Jensen, J. H., PROPKA3: Consistent Treatment of Internal and Surface Residues in Empirical pKa Predictions. *J. Chem. Theory Comput.* **2011,** *7*, 525-537.
9. Maier, J. A.; Martinez, C.; Kasavajhala, K.; Wickstrom, L.; Hauser, K. E.; Simmerling, C., ff14SB: Improving the Accuracy of Protein Side Chain and Backbone Parameters from ff99SB. *J. Chem. Theory Comput.* **2015,** *11*, 3696-3713.
10. Vanquelef, E.; Simon, S.; Marquant, G.; Garcia, E.; Klimerak, G.; Delepine, J. C.; Cieplak, P.; Dupradeau, F. Y., R.E.D. Server: a Web Service for Deriving RESP and ESP Charges and Building Force Field Libraries for New Molecules and Molecular Fragments. *Nucleic Acids Res.* **2011,** *39*, W511-7.
11. Wang, J.; Wolf, R. M.; Caldwell, J. W.; Kollman, P. A.; Case, D. A., Development and Testing of a General Amber Force Field. *J. Comput. Chem.* **2004,** *25*, 1157-1174.
12. Webb, B.; Sali, A., Comparative Protein Structure Modeling Using MODELLER. *Curr. Protoc. Bioinformatics* **2016,** *54*, 5.6.1-5.6.37.
13. Tooke, C. L.; Hinchliffe, P.; Bragginton, E. C.; Colenso, C. K.; Hirvonen, V. H. A.; Takebayashi, Y.; Spencer, J., β-Lactamases and β-Lactamase Inhibitors in the 21st Century. *J. Mol. Biol.* **2019,** *431*, 3472-3500.
14. Case, D. A.; Cerutti, D. S.; Cheatham, T. E. I.; Darden, T. A.; Duke, R. E.; Giese, T. J.; Gohlke, H.; Goetz, A. W.; Greene, D.; Homeyer, N.; Izadi, S.; Kovalenko, A.; Lee, T. S.; LeGrand, S.; Li, P.; Lin, C.; Liu, J.; Luchko, T.; Luo, R.; Mermelstein, D.; Merz, K. M.; Monard, G.; Nguyen, H.; Omelyan, I.; Onufriev, A.; Pan, F.; Qi, R.; Roe, D. R.; Roitberg, A.; Sagui, C.; Simmerling, C. L.; Botello-Smith, W. M.; Swails, J.; Walker, R. C.; Wang, J.; Wolf, R. M.; Wu, X.; Xiao, L.; D.M., Y.; P.A., K. *AMBER 2017*, University of California: San Francisco, 2017.
15. Walker, R. C.; Crowley, M. F.; Case, D. A., The Implementation of a Fast and Accurate QM/MM Potential Method in Amber. *J. Comput. Chem.* **2008,** *29*, 1019-1031.
16. Kästner, J., Umbrella Sampling. *WIREs Comput. Mol. Sci.* **2011,** *1*, 932-942.

17. Gaus, M.; Cui, Q.; Elstner, M., DFTB3: Extension of the Self-Consistent-Charge Density-Functional Tight-Binding Method (SCC-DFTB). *J. Chem. Theory Comput.* **2012,** *7*, 931-948.
18. Kumar, S.; Bouzida, D.; Swendsen, R. H.; Kollman, P. A.; Rosenberg, J. M., The Weighted Histogram Analysis Method for Free-Energy Calculations on Biomolecules. I. The Method. *J. Comput. Chem.* **1992,** *13*, 1011-1021.
19. Marcos-Alcalde, I.; Setoain, J.; Mendieta-Moreno, J. I.; Mendieta, J.; Gomez-Puertas, P., MEPSA: Minimum Energy Pathway Analysis for Energy Landscapes. *Bioinformatics* **2015,** *31*, 3853-3855.
20. Oueslati, S.; Nordmann, P.; Poirel, L., Heterogeneous Hydrolytic Features for OXA-48-like β-Lactamases. *J. Antimicrob. Chemother.* **2015,** *70*, 1059-1063.
21. Zhao, Y.; Truhlar, D. G., The M06 Suite of Density Functionals for Main Group Thermochemistry, Thermochemical Kinetics, Noncovalent Interactions, Excited States, and Transition Elements: Two New Functionals and Systematic Testing of Four M06-class Functionals and 12 Other Functionals. *Theor. Chem. Acc.* **2007,** *120*, 215-241.
22. Ditchfield, R.; Hehre, W. J.; Pople, J. A., Self-Consistent Molecular-Orbital Methods. IX. An Extended Gaussian-Type Basis for Molecular-Orbital Studies of Organic Molecules. *J. Chem. Phys.* **1971,** *54*, 724-728.
23. Lee, C.; Yang, W.; Parr, R. G., Development of the Colle-Salvetti Correlation-Energy Formula into a Functional of the Electron Density. *Phys. Rev. B Condens. Matter.* **1988,** *37*, 785-789.
24. Becke, A. D., Density-Functional Exchange-Energy Approximation with Correct Asymptotic Behavior. *Phys. Rev. A Gen. Phys.* **1988,** *38*, 3098-3100.
25. Frisch, M. J.; Trucks, G. W.; Schlegel, H. B.; Scuseria, G. E.; Robb, M. A.; Cheeseman, J. R.; Scalmani, G.; Barone, V.; Petersson, G. A.; Nakatsuji, H.; Li, X.; Caricato, M.; Marenich, A.; Bloino, J.; Janesko, B. G.; Gomperts, R.; Mennucci, B.; Hratchian, H. P.; Ortiz, J. V.; Izmaylov, A. F.; Sonnenberg, J. L.; Williams-Young, D.; Ding, F.; Lipparini, F.; Egidi, F.; Goings, J.; Peng, B.; Petrone, A.; Henderson, T.; Ranasinghe, D.; Zakrzewski, V. G.; Gao, J.; Rega, N.; Zheng, G.; Liang, W.; Hada, M.; Ehara, M.; Toyota, K.; Fukuda, R.; Hasegawa, J.; Ishida, M.; Nakajima, T.; Honda, Y.; Kitao, O.; Nakai, H.; Vreven, T.; Throssell, K.; Montgomery, J., J. A. ; Peralta, J. E.; Ogliaro, F.; Bearpark, M.; Heyd, J. J.; Brothers, E.; Kudin, K. N.; Staroverov, V. N.; Keith, T.; Kobayashi, R.; Normand, J.; Raghavachari, K.; Rendell, A.; Burant, J. C.; Iyengar, S. S.; Tomasi, J.; Cossi, M.; Millam, J. M.; Klene, M.; Adamo, C.; Cammi, R.; Ochterski, J. W.; Martin, R. L.; Morokuma, K.; Farkas, O.; Foresman, J. B.; Fox, D. J. *Gaussian 09, Revision D.01*, Gaussian, Inc.: Wallingford CT, 2016.
26. Kendall, R. A.; Dunning, T. H.; Harrison, R. J., Electron Affinities of the First-row Atoms Revisited. Systematic Basis Sets and Wave Functions. *J. Chem. Phys.* **1992,** *96*, 6796-6806.
27. Woon, D. E.; Dunning, T. H. J., Gaussian Basis Sets for Use in Correlated Molecular Calculations. III. The Atoms Aluminum Through Argon. *J. Chem. Phys.* **1993,** *98*, 1358-1371.
28. Gerenkamp, M.; Grimme, S., Spin-component Scaled Second-Order Møller–Plesset Perturbation Theory for the Calculation of Molecular Geometries and Harmonic Vibrational Frequencies. *Chem. Phys. Lett.* **2004,** *392*, 229-235.
29. Neese, F., The ORCA Program System. *WIREs Comput. Mol. Sci.* **2012,** *2*, 73-78.
30. Neese, F., Software Update: the ORCA Program System, Version 4.0. *WIREs Comput. Mol. Sci.* **2017,** *8*, e1327.
31. Weigend, F.; Köhn, A.; Hättig, C., Efficient Use of the Correlation Consistent Basis Sets in Resolution of the Identity MP2 Calculations. *J. Chem. Phys.* **2002,** *116*, 3175-3183.